Separation and Purification Technology 67 (2009) 187–193

Contents lists available at ScienceDirect

Separation and Purification Technology

journal homepage: www.elsevier.com/locate/seppur

Photocatalytic air purification: Comparative efficacy and pressure drop of a TiO_2-coated thin mesh and a honeycomb monolith at high air velocities using a 0.4 m^3 close-loop reactor

Jérôme Taranto[a,b,1], Didier Frochot[a], Pierre Pichat[b,*]

[a] EDF – Les Renardières, 77818 Moret-sur-Loing, France
[b] "Photocatalyse et Environnement", CNRS UMR "IFoS", STMS, Ecole Centrale de Lyon, 69134 Ecully CEDEX, France

ARTICLE INFO

Keywords:
Photocatalytic air purification
Methanol
Toluene
TiO_2 coatings
Air filters

ABSTRACT

Photocatalytic purifiers, which are in development for treating gaseous effluents at flow rates generally higher than several tens of $m^3\ h^{-1}$, usually employ TiO_2-coated materials either as planar or folded fibrous filters, or as honeycomb monoliths. Our primary objective was to compare the photocatalytic efficacy of two types of these materials using a *ca.* 0.4 m^3 close-loop, air tight, photocatalytic reactor we built at EDF. This loop – through which air can be flowed at rates from 16 to 1800 $m^3\ h^{-1}$, i.e. 0.11–12.25 $m\ s^{-1}$ – includes a paralleliped (560 mm × 295 mm × 200 mm) into which alternate banks of lamps and TiO_2 coated-materials (entrance area = 408 cm^2) can be accommodated. The materials tested were (i) an Ahlstrom-supplied, thin, non-woven tissue dried at room temperature after impregnation with both Degussa TiO_2 P-25 and colloidal SiO_2 used as a binder and (ii) an aluminum honeycomb-shaped material we coated with Degussa TiO_2 P-25 and dried at room temperature. U-shaped lamps emitting at 254 nm and having an electrical power of 18 or 35 W were employed. The geometries of the materials and the spatial arrangements of the lamps and materials provided an irradiance of the materials as high and homogeneous as possible according to our modeling [Catal. Today 122 (2007) 66–77]. Methanol was chosen as the test pollutant because it is easily mineralized, which minimized the inhibition of the photocatalytic activity by intermediate products. In the recirculation regime, the initial rates of methanol removal observed for the folded tissue were multiplied by at least four – depending on the numbers of materials and banks of three 35 W lamps – when the honeycomb material was utilized. Several factors can add to cause this high increase in efficacy: distinct shapes and TiO_2 supports, differences in photons scattering, and the reduced accessibility of reactants to TiO_2 because of SiO_2. Regarding energy consumption, the use of two photocatalytic materials sandwiching one bank of three 35 W lamps instead of one material in-between two banks of three lamps led to about the same efficacy. The honeycomb material was also tested with toluene at an initial concentration corresponding to the same amount of carbon as when methanol was the pollutant. The removal rate and CO_2 formation rate were lower for toluene than for methanol, which can be easily explained by a lower reactivity with respect to oxidation, a smaller adsorbed amount and a higher competition with the more numerous degradation intermediate products. That comparison illustrates the need of trials for every effluent to be treated. Considerable differences in pressure drop between the two materials clearly demonstrated another interest of using honeycomb shapes, at least for the materials and configurations investigated. Furthermore, a deactivation, together with a yellowing, was noticed at high irradiance for the Ahlstrom tissue, which included cellulose fibers. Folding the material enables one to employ lower irradiances for minimizing this effect, while maintaining the efficacy because of the increase in the material area in the reactor, as well as slightly lowering the pressure drop.

1. Introduction

Because of its oxidizing capacities with respect to chemical compounds and micro-organisms, photocatalysis over TiO_2 can be used to purify, deodorize and decontaminate air. That has led, in spite of problems not always properly considered [1–6], to the commercialization of indoor air photocatalytic cleaners. The pos-

* Corresponding author. Tel.: +33 4 78 66 05 50; fax: +33 4 78 33 11 40.
E-mail addresses: j.taranto@biowind.fr (J. Taranto), didier.frochot@edf.fr (D. Frochot), pichat@ec-lyon.fr (P. Pichat).
[1] Present address: BIOWIND, 36 rue Oberlin, 67000 Strasbourg, France.

1383-5866/$ – see front matter © 2009 Elsevier B.V. All rights reserved.
doi:10.1016/j.seppur.2009.03.017

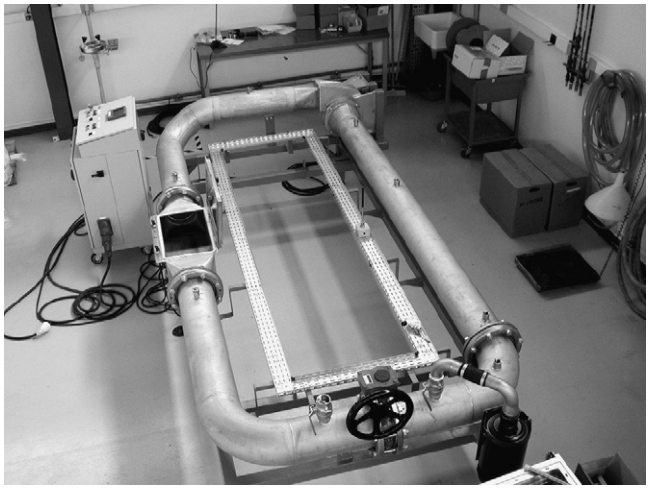

Fig. 1. Picture of the loop, the cover of the paralleliped photocatalytic reactor being removed.

sibility of efficiently treating air effluents depends on the case. General information on photocatalysis, including air treatment, can be found in a book [7] and recent reviews [1,3]. Photocatalytic air cleaning has been recently evaluated [8,9]. Relevant references until October 2001 are gathered in an organized bibliography [10].

To test TiO_2 coated-materials and UV lamps used for photocatalytic air purification, we have designed and built at EDF a *ca.* 0.4 m^3 close-loop reactor (Fig. 1), which is described in Section 2.1. This reactor enables airflow rates through the photocatalytic materials up to 1800 $m^3\ h^{-1}$ (12.25 $m\ s^{-1}$), which means that flow rates commonly used in photocatalytic purifiers can be attained. These rates are much higher than those employed in laboratory tests, however, with a few exceptions [2,4–6,11–13].

Although many photocatalytic reactor geometries and therefore configurations for the TiO_2-coated materials have been proposed, particularly in numerous patents [10], filter meshes [2,14–16] and honeycomb monoliths [4–6,11–13,17] are most often advocated. Accordingly, in a first stage, we have proposed a methodology for modeling and optimizing irradiance on planar, folded, and honeycomb shapes in order to maximize photocatalytic air purification [18].

Here, in a second stage, our main goal was to compare photocatalytic results obtained, using our close-loop reactor, with (i) a folded material made of a thin, non-woven tissue coated with both TiO_2 and SiO_2 used as a binder, and (ii) honeycomb-shaped aluminum coated with the same kind of TiO_2. These materials are described in Section 2.5. Their geometries and the spatial arrangements of the lamps and materials were those derived from the aforementioned modeling. This warranted that each material was tested under the most appropriate conditions and thereby that the comparison was not biased. For this comparison, methanol was selected because it can form only a small number of incompletely oxidized intermediate products; therefore, methanol removal rates are not significantly affected by these products [19,20]. By contrast, toluene was also used with the honeycomb material – which was found to be far more efficient than the folded material – in order to reveal the effects of both a more stable pollutant and numerous degradation intermediate products [21], at the same initial concentration in terms of carbon atoms. These comparisons of photocatalytic efficacies were complemented by pressure drop measurements for both types of materials and by a study of the stability of the tissue cellulose fibers depending on the value of the irradiance.

2. Experimental, materials and methods

2.1. Close-loop photocatalytic reactor

This reactor was designed and fabricated at EDF R&D. The close-loop consisted of stainless-steel tubes having an internal diameter of 219 mm (Fig. 1). It included a stainless-steel parallelepiped photocatalytic reactor whose dimensions are indicated in Fig. 2. The overall length and width of the close-loop were respectively 3 and 1.3 m, and the total air volume in the tubes, the reactor and the fan – placed outside the loop – was 0.377 m^3. The removable cover of the reactor included a 1 cm thick PVC window which allowed one to check, before each photocatalytic experiment, whether the lamps were operating properly while protecting the experimentalist from exposure to UV radiation. During the photocatalytic experiments, an additional stainless-steel plate was placed between the airtight joint and the cover, so that the reflection of light on the top was similar to that on the bottom of the reactor. Whatever its shape, the photocatalytic material was maintained inside the reactor by use of a stainless-steel holder (290 mm × 195 mm × 2 mm) which could be easily inserted in rails fixed to the reactor walls. An airtight joint surrounded this holder to force all the air to pass through the photocatalytic material whose entrance area was thus: 25.5 cm × 16.5 cm = 408 cm^2.

Appropriate stainless-steel supports permitted one to change both the space between the lamps and the distance between the photocatalytic material and the lamps which were placed vertically. Inside the reactor the electrical wires were wrapped with aluminum foil to prevent exposure of their polymeric coatings to UV radiation. The ballasts of the lamps were outside the loop.

The airflow velocity was controlled by a speed adjuster acting on the fan and measured by use of a Höntzsch thermal flow sensor. When the parallelepiped reactor was completely empty, the maximum airflow rate was higher than 2000 $m^3\ h^{-1}$ (i.e., a velocity over 14.6 $m\ s^{-1}$). Before each photocatalytic experiment, to remove TiO_2 particles which could have been detached from the photocatalytic material used in the previous run, the reactor and lamps were manually cleaned, and air at the maximum velocity was passed through the open loop for several minutes. The air admitted into the loop was passed through a particle filter. The treated air was filtered with an activated carbon filter to remove residual methanol or toluene and possibly degradation intermediate products before rejection into the atmosphere.

2.2. UV lamps and light measurements

PL-L TUV Philips low-pressure mercury lamps emitting mainly at 254 nm were used. These lamps comprise two joint parallel tubes each having an external diameter of 17 mm, which corresponds to an overall external diameter of 37 mm for the lamp; the total lamp length including the electrical base is 225 mm. The electrical power

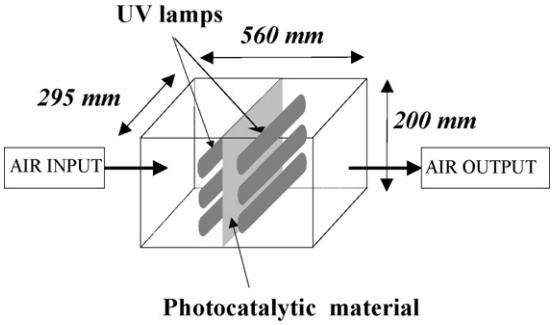

Fig. 2. Scheme of the photocatalytic reactor.

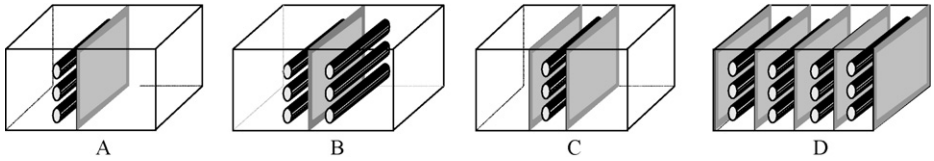

Fig. 3. Scheme showing the various arrangements of UV lamps and photocatalytic materials used.

is either 18 or 35 W. The emitted UV power is highest between 313 and 353 K, which is close enough to the temperature range of ambient air.

For measuring the UV lamps output as a function of wavelength, a Solatell Sola Scope 2000 spectroradiometer was used. This apparatus was wavelength and irradiance calibrated for absolute measurement.

For irradiance measurements, we utilized an International Light IL1700 radiometer and an IL1771 sensor specially designed for lighting sources emitting at 254 nm. The irradiance was measured at 63 points of the planar irradiated material (Section 3.4), these points being separated by 25 mm from one another.

2.3. Introduction of methanol or toluene into the loop. Concentration measurements

A device (Maihak Company) comprising a syringe, a manual valve, a mass flowmeter and a stainless-steel chamber was employed to contaminate air with methanol or toluene. The syringe enabled one to introduce a known amount of the liquid pollutant into the chamber whose temperature was adjusted in order to rapidly vaporize this organic compound. The vapor was carried out of the chamber by air pumped at a constant rate from the loop, and introduced into the loop via an appropriately heated rod. Air was then circulated for one hour before the lamps were switched on.

The methanol or toluene concentration was monitored by use of an Innova Photoacoustic Multi-gas Monitor 1312 equipped with appropriate filters depending on the compound, as well as a filter that enables compensation for interference from water vapor. To measure the amount of CO_2 formed, we used a Varian micro-gas chromatograph CP-2003 which included a thermal conductivity detector and a capillary column (1.04 m long; 0.7 mm internal diameter).

2.4. Pressure drop measurements

The pressure drop measurements were performed with an Auxitrol Smart atmospheric pressure sensor and electronic transmitter connected to a Dieterich Standard Dart II single-run flow computer for differential-pressure metering. They were recorded on each side of the photocatalytic reactor and close to it, that is, as far away as possible from the tube bends (Fig. 1) to minimize the influence of turbulence.

2.5. TiO_2-coated materials

2.5.1. Fibrous material

TiO_2 was affixed on a thin non-woven tissue (80 g m^{-2}) made of cellulose fibers (Ahlstrom reference: NW) by means of a "size press" using a mixture containing powder Degussa TiO_2 P-25 and an aqueous colloidal suspension of SiO_2 (particle size = 20–30 nm; TiO_2/SiO_2 mass ratio = 1; TiO_2 mass = 18.5 g m^{-2} of tissue) used to better bind the TiO_2 particles to the fibers. The impregnated tissue was allowed to dry at room temperature [22].

2.5.2. Honeycomb-shaped material

Aluminum honeycomb-shaped materials were purchased from Goodfellow. The cells are hexagonal. To optimize the irradiance of the honeycomb material, we used in the photocatalytic tests reported here the geometry that was found to be the best according to our modeling [18], viz. cells radius = 6.4 mm (in the model, the irregular hexagons having two sides of 5.5 mm and four sides of 6.2 mm were assimilated to circles); honeycomb length = 40 mm (see also Section 3.2).

The honeycomb material was first cleaned by dipping it for 15 min in a 42 kHz ultrasound bath containing demineralized water. The honeycomb material was then dipped into another 42 kHz ultrasound bath containing an aqueous suspension of 5 wt% TiO_2 Degussa P-25. Sonication was initially activated for 1 h to homogenize the suspension and then for 2 min between each TiO_2 deposition (*vide infra*). To avoid thicker deposition of TiO_2 in the lower part of the honeycomb cells, a jet of air at a pressure of 2×10^5 Pa was then forced four times through the honeycomb material removed from the bath, alternatively from one side and from the other, the honeycomb material being rotated by 45° each time. That procedure allowed us to obtain a visually evenly deposited layer of TiO_2. The whole depositing process was repeated 10 times to reach, after drying at room temperature, a layer of *ca.* 4 g m^{-2}, which was determined to be optimal for the photocatalytic removal of methanol from air [23].

Before use in the close-loop reactor, the honeycomb material was submitted to mechanical strains similar to those corresponding to its handling by the experimentalist; the resulting TiO_2 losses were lower than 6 wt%. Additional TiO_2 losses due to the subsequent photocatalytic tests at an air velocity of 0.34 m s^{-1} were estimated to be on the order of 1 wt%. According to previous studies [24,25], TiO_2 adhesion on aluminum can be improved by electrochemically forming an alumina layer. In the present case, dipping the honeycomb material into aqueous solutions of the acids HCl, HNO_3, H_2SO_4 or H_3PO_4, even at very low concentrations, produced an unacceptable weakening of the mechanical properties of the material because of the thin walls (64 μm thick) of the honeycomb cells.

3. Results and discussion

3.1. Comparison of the efficacy of the two types of materials (folded and honeycomb)

The efficacy of the two types of folded and honeycomb materials described in Section 2.5. has been compared. To that end, the optimal irradiance conditions – viz. geometry of the materials, distance between the lamps and the material, and space between the lamps, derived from our modeling [18] – were used. Banks of three 35 W lamps were employed and the arrangements utilized in the photocatalytic tests are shown in Fig. 3. The pollutant used for comparing the folded and honeycomb materials was methanol. Figs. 4 and 5 show that, depending on the arrangement (Fig. 3), the initial rates of methanol removal were at least 4 times faster for the honeycomb material than for the folded material utilized. The quantity of affixed TiO_2 Degussa P-25 present in the reactor (2.04 g for the honeycomb and 1.05 g for the folded material) might be considered as one of the causes of this difference in efficacy. However, the

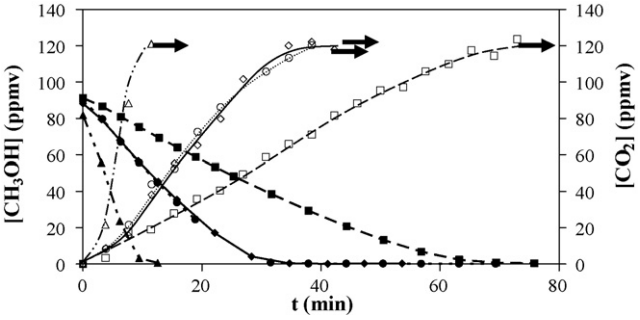

Fig. 4. Variations in CH_3OH and CO_2 concentrations against UV-irradiation time. The CH_3OH amount injected into the loop corresponded to a concentration of 100 ppmv (*ca.* 133.5 mg m^{-3} or *ca.* 4 mmol m^{-3}). The airflow rate was 50 m^3 h^{-1} or 0.34 m s^{-1} (recirculation regime). Squares: Three lamps, one material (see Fig. 3A). Circles: six lamps, one material (see Fig. 3B). Diamonds: three lamps, two materials (see Fig. 3C). Triangles: 12 lamps, five materials (see Fig. 3D). Distance between the lamps and the middle of the folds of the TiO_2-coated material = 42 mm; space between the lamps = 61 mm; angle of the folds = 91°; length of the fold side = 10 mm [18].

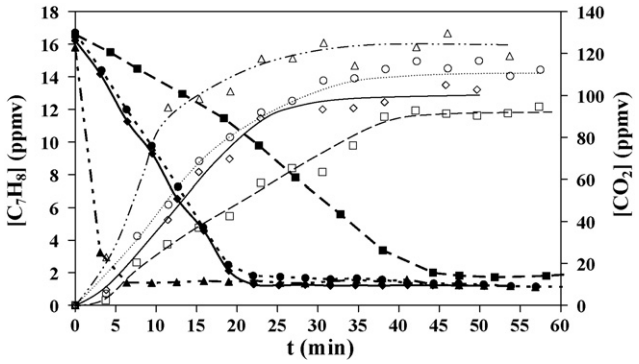

Fig. 6. As Fig. 5 for toluene instead of methanol. The toluene amount injected into the loop corresponded to a nominal concentration of 14.3 ppmv (*ca.* 55 mg m^{-3} or *ca.* 0.6 mmol m^{-3}); the higher initial concentration measured as well as the apparent residual concentration arose from an artifact in the measurement apparatus, which shifted the concentration values.

TiO_2 mass per area unit of solid support corresponded to a thickness beyond which no further increase in photocatalytic rates is observed because of the limited penetration depth of UV radiation in TiO_2 [23,26]. Consequently, the quantity of TiO_2 in each type of material cannot account for the difference in efficacy. In addition, both types of coatings were obtained by mere drying at room temperature, so that no detrimental thermal effect on the TiO_2 P-25 photocatalytic activity could occur in either case, and be at the origin of the efficacy difference for methanol removal. Our modeling [18] provided the geometric conditions for an optimum irradiation of the coating without any assumption on the optical and photocatalytic properties of the coating. Even though the TiO_2 was the same, the scattering of light was certainly different with the folded material and the honeycomb material used here because (i) SiO_2 was added to TiO_2 in the case of the folded material and (ii) reabsorption of initially scattered photons depends on the material shape. Above all, in a previous paper [27], one of us has shown by scanning electron microscopy-energy dispersive X-ray microanalysis (SEM-EDX) that the Ti/Si atomic ratio – SiO_2 was used as a binder – at the surface of the Ahlstrom coatings is lower than the nominal ratio, indicating that TiO_2 is partially covered by SiO_2. Furthermore, $^{18}O_2$–$Ti^{16}O_2$ isotopic exchange measurements under UV-irradiation [27] have clearly shown that TiO_2 in these coatings is poorly accessible to O_2 despite the small size of this molecule. Accordingly, we conclude here that, in addition to the role of the material shape, the use of silica as a binder caused the efficacy of the folded material to be much lower than that of the honeycomb material for methanol removal.

The energy consumption being proportional to the number of lamp banks, it is obvious that the ratio of the number of photocatalytic materials over the number of lamps banks should be as high as possible. Indeed, in our tests, arrangement C (two materials for one lamp bank) in Fig. 3 led to an efficacy not only higher than that of arrangement A (one material for one lamp bank) as expected, but even equivalent to arrangement B (one folded material for two lamp banks) or only slightly lower (one honeycomb material for two lamp banks) despite using only half the electrical power (Figs. 4 and 5). Furthermore, in going from arrangement B (one material for two lamp banks) to D (five materials for four lamp banks), that is, in only doubling the number of lamps, the methanol removal initial rate was increased by a factor markedly higher than two, particularly for the honeycomb material, owing to the use of five photocatalytic materials instead of one.

The curves in Figs. 4 and 5 show that the formation of CO_2 was almost complete when all the methanol in the closed-loop reactor had been eliminated. In other words, and not surprisingly, the efficacy for total mineralization of methanol correlated well with the efficacy for methanol removal for both kinds of photocatalytic materials and all numbers of lamps and materials (Fig. 3). That observation supports the choice of methanol as a pollutant that does not produce stable organic degradation products as mentioned in Section 1. Nevertheless, the shape of the CO_2-formation curves (with a convexity initially turned to the time axis) indicates the existence of intermediate degradation products. Note that the final concentration of CO_2 was higher than that expected from the complete mineralization of methanol. The Ahlstrom material contains cellulose fibers (see Sections 2.5.1 and 3.4) and synthetic polymers used to bind the fibers together. The aluminum sheets of the honeycomb material are joined by a resin. These organic substances can unfortunately generate CO_2 in the presence of UV light and TiO_2.

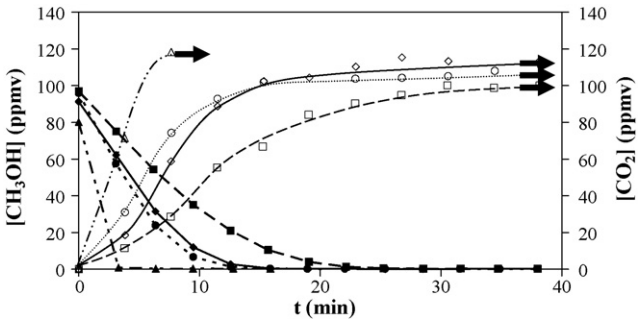

Fig. 5. As Fig. 4, but relating to the honeycomb material with the following characteristics: distance between the lamps and the cells entrance = 49 mm; space between the lamps = 52 mm; honeycomb length = 40 mm; cell radius = 6.4 mm [18].

3.2. Comparison of the efficacy of the honeycomb material for toluene or methanol removal and mineralization

The removal of toluene was also investigated in the close-loop reactor (Fig. 6) with the same arrangements of lamps and honeycomb materials (Fig. 3) as in the case of methanol. The initial toluene concentration admitted in the reactor was chosen so as to correspond to the same amount of carbon as that contained in methanol. Comparison of Figs. 5 and 6 shows that both the removal rate and CO_2 formation rate were lower for toluene than for methanol irrespective of the numbers of banks of lamps and honeycomb materials used. This observation is in line with a previous study showing a much higher apparent quantum yield for the photocatalytic removal of methanol than for that of toluene in the 100–200 ppmv concentration range [28]. Also, note that toluene is adsorbed on TiO_2 in lower amounts than methanol [29]. Moreover,

a change in the slope of the kinetic curve of toluene removal was found for the conditions corresponding to the lowest efficacy. This change was gradually attenuated for higher-efficacy conditions. These observations can both be interpreted as due to the fact that the multiple intermediate products of toluene degradation compete with toluene for adsorption and/or reaction with active species generated by TiO_2 photo-excitation. By contrast, as mentioned in Section 3.1., the intermediate products of methanol degradation (methanol, methanoic acid and methyl methanoate) are more easily oxidized or desorbed; the TiO_2 surface is hence more rapidly freed for methanol adsorption and oxidation.

These comparisons clearly illustrate the fact that for a given photocatalytic reactor the airflow rate must be adapted to the influent content in pollutants (nature and concentration) and to the expected purification level of the effluent. That requires trials for every case and/or calculations based on previous data. The size of the reactor and/or the number of lamps and area of photocatalytic material should also be changed, if needed, to meet the purification specifications. Modular photocatalytic reactors are hence advocated.

It can also be recalled here that the honeycomb used (see Section 2.5.2.) on the basis of our modeling [18] had a length over equivalent cell-diameter ratio of about 3. This value is roughly the limit to obtain full utilization of the incident flux for one-side irradiation [12]. A radiation field calculation in a honeycomb reactor by use of the Monte-Carlo method has recently confirmed that the photon absorption efficiency does not increase significantly when this ratio is "higher than approximately 2–3" [30].

3.3. Comparison of the pressure drops induced by the folded and honeycomb materials

The comparison of the two types of materials would not be complete if the pressure drop were not considered. In the photocatalytic tests discussed in Sections 3.1 and 3.2. (Figs. 4–6), the air flow rate was 50 $m^3\ h^{-1}$ corresponding to a velocity of 0.34 $m\ s^{-1}$. At this rate, given the 0.219 m inner diameter of the loop tubes, the Reynolds number was 6210. This value indicates a turbulent flow, which cannot be easily modeled. Therefore, we measured the pressure drops for the various arrangements (Fig. 3) and the two types of photocatalytic materials tested. From Fig. 7 showing pressure drops at various airflow rates, it clearly appears that the pressure drop, which was almost nil in the absence of lamps and photocatalytic materials, increased much more in the presence of folded materials than in that of honeycomb-shaped materials for the same number of three lamp banks and materials (Fig. 3). Indeed, the pressure drop produced by a three lamp bank was negligible relative to that produced by a folded material (Fig. 7A), whereas the pressure drop due to a honeycomb-shaped material was not much higher than that due to a three lamp bank (Fig. 7B). All pressure drops increased as a function of the flow rate according to a second-degree polynomial. For the highest airflow rate used (1800 $m^3\ h^{-1}$ or 12.25 $m\ s^{-1}$), the pressure drop was about 25 times as high for one folded material as for one honeycomb-shaped material. These measurements convincingly illustrate the interest of using honeycomb-shaped materials rather than the folded materials to achieve a lower pressure drop, at least for the materials and configurations investigated.

3.4. Stability of the TiO_2-coated fibrous material

The Ahlstrom thin, non-woven tissue used in this study is made of intertwined cellulose fibers. Cellulose is sensitive to UV irradiation and, like almost all organic compounds, prone to be degraded by photocatalysis. It may be thought to be protected to some extent by the photo-inactive silica used to bind TiO_2 to the tissue. But, as

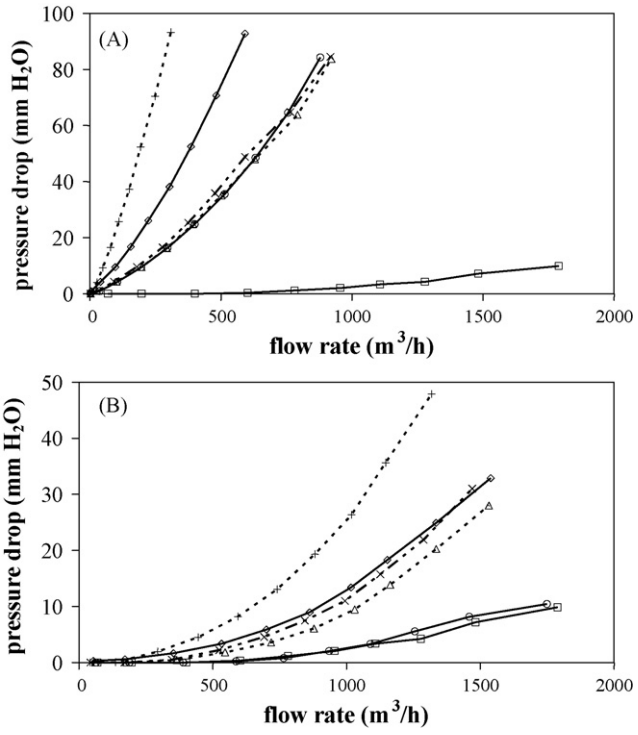

Fig. 7. Pressure drop against airflow rate: (A) folded material; (B) honeycomb-shaped material. Squares: three lamps. Circles: one material. Triangles: three lamps, one material (see Fig. 3A). Multiplication signs: six lamps, one material (see Fig. 3B). Diamonds: three lamps, two materials (see Fig. 3C). Addition signs: 12 lamps, five materials (see Fig. 3D).

mentioned in Section 3.1., there is more SiO_2 in the top layers of the coating than in the bottom layers near the cellulose support [27], which means that very likely a large fraction of TiO_2 is in contact with the cellulose fibers. Consequently, it was deemed of interest to test the stability of this TiO_2-coated material under UV irradiation. For that purpose, we studied the photocatalytic removal of methanol using the nonfolded material as a function of the average irradiance when 1–3 lamps having an electrical power of either 18 or 35 W were utilized. The average irradiance was measured as indicated in Section 2.2.

A linear relationship was found between the methanol removal rate and the irradiance up to *ca.* 60 $W\ m^{-2}$ (Fig. 8). However, for the highest irradiance used (108 $W\ m^{-2}$), a substantial decrease in the rate was observed to the point that the rate with the three 35 W lamps producing this irradiance was lower than with one

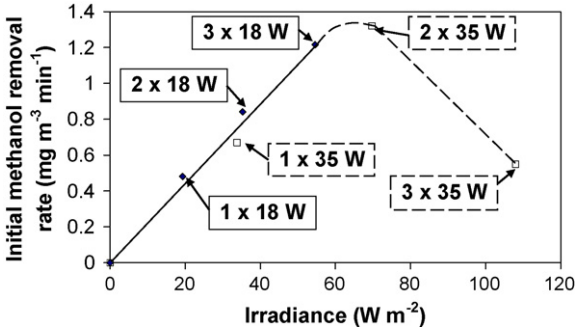

Fig. 8. Initial rate of methanol removal against the irradiance measured at the level of the planar TiO_2-coated material. The number and electrical power of the lamps were those indicated. The methanol amount injected into the loop corresponded to a concentration of 100 ppmv. Airflow rate = 50 $m^3\ h^{-1}$ (0.34 $m\ s^{-1}$). Distance between the lamp(s) and the TiO_2-coated material = 77 mm; space between the lamps = 62.5 mm.

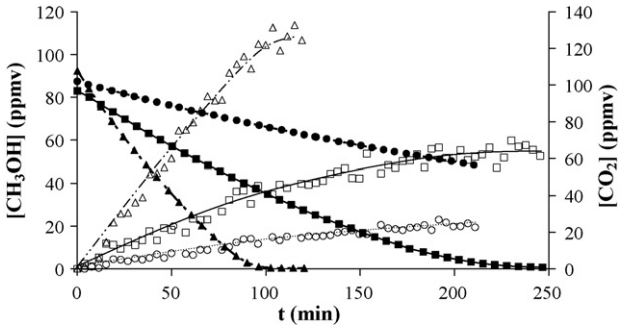

Fig. 9. Variations in CH_3OH and CO_2 concentrations against UV-irradiation time for the planar TiO_2-coated material. Three 35 W lamps were used. Other conditions as in Fig. 8. Triangles: non-UV-pretreated material. Squares: overnight UV-pretreated material. Circles: experiment using the overnight UV-pretreated material a second time.

35 W lamp and not much higher than with one 18 W lamp. This can be attributed only to a deactivation of the photocatalytic material, since a predominance of the recombination rate of the photogenerated charges – caused by the increase in irradiance – would only make the methanol removal rate become proportional to the irradiance square root [31], but not diminish. Indeed, the results of Fig. 9 confirm the deactivation, since when three 35 W lamps were employed (i) a reused material was much less efficient and (ii) an overnight UV-pretreated material (in the absence of methanol) was markedly less efficient than a nonpretreated material. Besides, the photocatalytic material submitted to the irradiation of three 35 W lamps became yellowish, thus evidencing its alteration. Light-induced yellowing of cellulose and other organic polymers is a well-known phenomenon [32,33]. In the present case, the cellulose fibers are coated by highly UV-absorbing TiO_2 particles, but the coverage may not be perfectly continuous and the SiO_2 particles, mixed with the TiO_2 particles, do not absorb at 254 nm, so that it cannot be excluded that a fraction of the UV irradiation reaches the fibers and thereby can alter them photochemically. In addition, irradiance-dependent photocatalysis is expected to degrade cellulose, as aforementioned. It is conceivable that the cellulose degradation products compete with methanol for the photocatalytically generated active species, which explains the decrease in methanol removal rate.

These results show that the choice of cellulose fibers as a support to TiO_2 particles, while economically interesting and environmentally friendly, limits both the time during which the material remains fully efficient and the value of the irradiance that can be used. One possibility of diminishing the irradiance in order to minimize cellulose degradation without affecting the photocatalytic efficacy for air purification is to counterbalance the decrease in TiO_2 photo-excitation by an increase in the area of TiO_2-coated material present in the reactor. That objective can be reached by folding the material. That is one of the reasons why the photocatalytic experiments described in Section 3.1. were carried out with folded fibrous materials. Indeed, measurements showed that the methanol removal rate did not significantly change when the planar material was folded; in these measurements, the angle of folds varied from 24° to 113° and the length of folds sides from 6 to 12 mm, with these values being the limits selected in our modeling of the irradiance of the folded material [18]. Note that the area of the face of the material through which the air was flowed remained the same (408 cm^2).

Moreover, measurements showed that the pressure drop was lower – e.g., by about 5% at *ca.* 800 $m^3\ h^{-1}$ or 5.45 $m\ s^{-1}$ (the highest flow rate that can be operated under these conditions) – when the material was folded (folds angle = 91°; length of sides = 10 mm as in Section 3.1 [18]) instead of being planar. This lower pressure drop is an additional reason for folding the material in this type of air purifier.

4. Conclusions

First, these results illustrate that the appropriately equipped loop reactor we built allows one to compare lamps, photocatalytic materials and chemical pollutants regarding both the photocatalytic activity and the pressure drop.

Second, our method for depositing powder in an aluminum honeycomb leads to a non-thermally-treated coating that withstands high air velocities and exhibits a much higher photocatalytic efficacy for methanol removal than a thin fibrous tissue onto which TiO_2 is affixed with the use of SiO_2, at least in the recirculation regime at the methanol initial concentration (100 ppmv) and airflow rates (50 $m^3\ h^{-1}$ or 0.34 $m\ s^{-1}$) we used.

Third, the considerably lower pressure drop we measured through the honeycomb-shaped material relative to the thin fibrous tissue – even if it is folded – can permit sizable savings in the electrical energy used to operate the fans.

Fourth, we have shown that the use of cellulose fibers as a support for TiO_2 particles limits the photocatalytic efficacy by reducing the value of the irradiance that can safely be employed without causing deactivation due to photo-induced damage to the material.

Acknowledgment

J.T. is grateful to the ANRT for its contribution to his Ph. D. scholarship.

References

[1] P. Pichat, Photocatalytic degradation of pollutants in water and air: basic concepts and applications, in: M.A. Tarr (Ed.), Chemical Degradation Methods for Wastes and Pollutants: Environmental and Industrial Applications, Marcel Dekker, Inc., New York/Basel, 2003, pp. 77–119.
[2] J. Disdier, P. Pichat, D. Mas, Measuring the effect of photocatalytic purifiers on indoor air hydrocarbons and carbonyl pollutants, J. Air Waste Manage. Assoc. 55 (2005) 88–96.
[3] A.G. Agrios, P. Pichat, An overview of the state of the art and perspectives on materials and applications of photocatalysis over TiO_2, J. Appl. Electrochem. 35 (2005) 655–663.
[4] A.T. Hodgson, D.P. Sullivan, W.J. Fisk, Evaluation of ultra-violet photocatalytic oxidation (UVPCO) for indoor air applications: conversion of volatile organic compounds at low part-per-billion concentrations A, Lawrence Berkeley National Laboratory Report, LBNL-58936, 2005, pp. 1–64.
[5] A.T. Hodgson, D.P. Sullivan, W.J. Fisk, Evaluation of ultra-violet photocatalytic oxidation for indoor air applications, Lawrence Berkeley National Laboratory Report, LBNL-59631, 2006, pp. 1–8.
[6] A.T. Hodgson, H. Destaillats, T. Hotchi, W.J. Fisk, Evaluation of a combined ultraviolet photocatalytic oxidation (UVPCO)/chemisorbent air cleaner for indoor air applications, Lawrence Berkeley National Laboratory Report, LBNL-62202, 2007, pp. 1–74.
[7] M. Kaneko, I. Okura (Eds.), Photocatalysis: Science and Technology, Kodansha Springer, Tokyo, Berlin, 2002.
[8] D.T. Tompkins, B.J. Lawnicki, W.A. Zeltner, M.A. Anderson, Evaluation of photocatalysis for gas-phase air cleaning. Part 1. Process, technical and sizing considerations, ASHRAE Trans. 111 (2005) 60–84.
[9] D.T. Tompkins, B.J. Lawnicki, W.A. Zeltner, M.A. Anderson, Evaluation of photocatalysis for gas-phase air cleaning. Part 2. Economics and utilization, ASHRAE Trans. 111 (2005) 86–96.
[10] D.M. Blake, Bibliography of work on the heterogeneous photocatalytic removal of hazardous compounds from water and air, Update number 4 to October 2001, National Renewable Energy Laboratory Report, NREL/TP-570-26797, National Technical Information Service (NTIS), Springfield, VA (http://www.nrel.gov/docs/fy02osti/31319.pdf).
[11] R.J. Hall, P. Bendfeldt, T.N. Obee, J.J. Sangiovanni, Computational and experimental studies of UV/titania photocatalytic oxidation of VOCs in honeycomb monoliths, J. Adv. Oxid. Technol. 3 (1998) 243–252.
[12] Md.M. Hossain, G.B. Raupp, S.O. Hay, T.N. Obee, Three-dimensional developing flow model for photocatalytic monolith reactors, AIChE J. 45 (1999) 1309–1321.
[13] S.O. Hay, T.N. Obee, The augmentation of UV photocatalytic oxidation with trace quantities of ozone, J. Adv. Oxid. Technol. 4 (1999) 209–212.
[14] H. Ibrahim, H. de Lasa, Novel photocatalytic reactor for the destruction of airborne pollutants. Reaction kinetics and quantum yields, Ind. Eng. Chem. Res. 38 (1999) 3211–3217.

[15] J.E.O. Lopez, W.A. Jacoby, Microfibrous mesh coated with titanium dioxide: a self-sterilizing, self-cleaning filter, J. Air Waste Manage. Assoc. 52 (2002) 1206–1213.
[16] C.R. Esterkin, A.C. Negro, O.M. Alfano, A.E. Cassano, Air pollution remediation in a fixed bed photocatalytic reactor coated with TiO_2, AIChE J. 51 (2005) 2298–2310.
[17] M.L. Sauer, D.F. Ollis, Photocatalyzed oxidation of ethanol and acetaldehyde in humidified air, J. Catal. 158 (1996) 570–582.
[18] J. Taranto, D. Frochot, P. Pichat, Modeling and optimizing irradiance on planar, folded, and honeycomb shapes to maximize photocatalytic air purification, Catal. Today 122 (2007) 66–77.
[19] J. Taranto, D. Frochot, P. Pichat, Combining cold plasma and TiO_2 photocatalysis to purify gaseous effluents: a preliminary study using methanol-contaminated air, Ind. Eng. Chem. Res. 46 (2007) 7611–7614.
[20] P. Pichat, H. Courbon, R. Enriquez, T.T.Y. Tan, R. Amal, Light-induced isotopic exchange between O_2 and semiconductor oxides, a characterization method that deserves not to be overlooked, Res. Chem. Intermed. 33 (2007) 239–250.
[21] O. d'Hennezel, P. Pichat, D.F. Ollis, Benzene and toluene gas-phase photocatalytic degradation over H_2O and HCl pretreated TiO_2: by-products and mechanisms, J. Photochem. Photobiol. A: Chem. 118 (1998) 197–204.
[22] F.-P. Navarre, B. Bossand, P. Girard, J. Dussaud, Filled Paper for Gas Filtration, US Patent 5,965,091 (1999).
[23] J. Taranto, Etude des effets de paramètres influençant l'efficacité d'un épurateur photocatalytique d'air. Modélisation et optimisation de l'éclairement sur des matériaux photocatalytiques plans, plissés et en nid d'abeilles, Ph.D. Dissertation, Ecole Centrale de Lyon, Ecully, France, 2005.
[24] Y. Ishikawa, Y. Matsumoto, Electrodeposition of TiO_2 photocatalyst into nanopores of hard alumite, Electrochim. Acta 46 (2001) 2819–2824.
[25] Y. Ishikawa, Y. Matsumoto, Electrodeposition of TiO_2 photocatalyst into porous alumite prepared in phosphoric acid, Solid State Ionics 151 (2002) 213–218.
[26] N. Negishi, S. Matsuzawa, K. Takeuchi, P. Pichat, Transparent μm-thick TiO_2 films on SiO_2-coated glass prepared by repeated dip-coating/calcination: characteristics and photocatalytic activities for removing acetaldehyde or toluene in air, Chem. Mater. 19 (2007) 3808–3814.
[27] R. Enriquez, B. Beaugiraud, P. Pichat, Mechanistic implications of the effect of TiO_2 accessibility in TiO_2–SiO_2 coatings upon chlorinated organics photocatalytic removal in water, Water Sci. Technol. 49 (2004) 147–152.
[28] E. Berman, J. Dong, Photocatalytic decomposition of organic pollutants in gas streams, Chem. Oxid. 3 (1994) 183–189.
[29] R.M. Alberici, W.F. Jardim, Photocatalytic destruction of VOCs in the gas-phase using titanium dioxide, Appl. Catal. B 14 (1997) 55–68.
[30] M. Singh, I. Salvado-Estivill, G. Li Puma, Radiation field optimization in photocatalytic monolith reactors for air treatment, AIChE J. 53 (2007) 678–686.
[31] T.A. Egerton, C.J. King, The influence of light intensity on photoactivity in TiO_2 pigmented systems, J. Oil Colour Chem. Assoc. 62 (1979) 386–391.
[32] C. Heitner, J.C. Scaiano (Eds.), Photochemistry of lignocellulosic materials, Amer. Chem. Soc., Symp. Ser., 1993.
[33] L. Campanella, M. Battilotti, C. Costanza, Studies on simulated ageing of paper by photochemical degradation, Ann. Chim. 11 (1995) 727–740.